This document was prepared in conjunction with work accomplished under Contract No. DE-AC09-96SR18500 with the U. S. Department of Energy.

DISCLAIMER

This report was prepared as an account of work sponsored by an agency of the United States Government. Neither the United States Government nor any agency thereof, nor any of their employees, makes any warranty, express or implied, or assumes any legal liability or responsibility for the accuracy, completeness, or usefulness of any information, apparatus, product or process disclosed, or represents that its use would not infringe privately owned rights. Reference herein to any specific commercial product, process or service by trade name, trademark, manufacturer, or otherwise does not necessarily constitute or imply its endorsement, recommendation, or favoring by the United States Government or any agency thereof. The views and opinions of authors expressed herein do not necessarily state or reflect those of the United States Government or any agency thereof.

This report has been reproduced directly from the best available copy.

Available for sale to the public, in paper, from: U.S. Department of Commerce, National Technical Information Service, 5285 Port Royal Road, Springfield, VA 22161,
phone: (800) 553-6847,
fax: (703) 605-6900
email: orders@ntis.fedworld.gov
online ordering: http://www.ntis.gov/help/index.asp

Available electronically at http://www.osti.gov/bridge
Available for a processing fee to U.S. Department of Energy and its contractors, in paper, from: U.S. Department of Energy, Office of Scientific and Technical Information, P.O. Box 62, Oak Ridge, TN 37831-0062,
phone: (865)576-8401,
fax: (865)576-5728
email: reports@adonis.osti.gov

Mechanisms of Strontium and Uranium Removal from High-level Radioactive Waste Simulant Solutions by the Sorbent Monosodium Titanate

M. C. Duff [1,*], D. B. Hunter [1], D. T. Hobbs [1], S. D. Fink [1], Z. Dai [2,3], and J. P. Bradley [2,3]

[1] Westinghouse Savannah River Company (WSRC), Savannah River Technology Center (SRTC), Aiken, SC 29808. * Corresponding author.

[2] MVA Incorporated, 5500 Oakbrook Parkway, Norcross, GA, 30093, USA.

[3] Presently with Lawrence Livermore National Laboratory, Livermore, CA, 94551, USA.

Abstract

High-Level Waste (HLW) is a waste associated with the dissolution of spent nuclear fuel for the recovery of weapons-grade material. It is the priority problem for the U.S. Department of Energy's Environmental Management Program. Current HLW treatment processes at the Savannah River Site (Aiken, SC) include the use of monosodium titanate (MST, with a similar stoichiometry to $NaTi_2O_5.xH_2O$) to concentrate strontium (Sr) and actinides. The high affinity of MST for Sr and actinides in HLW solutions rich in Na^+ is poorly understood. Mechanistic information about the nature of radionuclide uptake will provide insight about MST treatment reliability. Our study characterized the morphology of MST and the chemistry of sorbed Sr^{2+} and uranium [U(VI)] as uranyl ion, UO_2^{2+}, on MST, which were added (individually) from stock solutions of Sr and $^{238}U(VI)$ with spectroscopic and transmission electron microscopic techniques. The local structural speciation of sorbed U varied with loading and but not for Sr. Sorbed Sr exhibited specific adsorption as partially-hydrated species whereas sorbed U exhibited specific adsorption as monomeric and dimeric U(VI)-carbonate complexes. Sorption proved site specific. These differences in site specificity and sorption mechanism may account for the difficulties associated with predicting Sr and U loading and removal kinetics using MST.

Introduction

High-Level Waste (HLW) is a radioactive waste associated with the dissolution of spent nuclear fuel rods for the recovery of weapons grade material. At the Savannah River Site (SRS, Aiken, SC), nearly 130 million L of HLW await disposition. This waste is highly alkaline, concentrated in Na^+ and NO_3^- (added to prevent tank corrosion). The waste is stored in three typical

forms: sludge, salt cake and salt solution. Treatment of the waste will involve dissolving the salt cake and concentrating the actinides, radiocesium and radiostrontium from the solution followed by vitrification of the waste concentrate. Several sorbent materials such as silicate clays, metal oxides have high affinities for radionuclides in aqueous solutions.[1,2,3,4,5,6] Titanate solids such as monosodium titanate (MST, with a similar stoichimetry to $NaTi_2O_5.xH_2O$ where x is unknown) and sodium nonatitanate ($Na_4Ti_9O_{20}.xH_2O$) are chemically stable in high pH solutions. These materials show great promise for use in the removal of radiostrontium (mainly ^{90}Sr) and actinides [uranium (U), plutonium (Pu) and neptunium (Np)] under conditions that are relevant to the processing of highly alkaline salt solutions.[6,7]

The current designs for the Salt Processing Facility at the SRS include the use of MST for Sr and actinide removal during HLW treatment. Also, the Actinide Removal Process will start radioactive operation in early 2004 using this chemistry. However, the fundamental mechanisms for removal of Sr and actinides remain unknown. On the atomic level, the removal of metals from solution by surfaces can occur via several fundamental mechanisms such as structural incorporation, ion exchange (including electrostatic or outer-sphere) sorption, specific (or inner sphere) adsorption and surface precipitation/polymerization. [A review of these processes is presented elsewhere.[8]] In some cases, more than one mechanism may operate (for example specific adsorption and surface precipitation. Therefore, personnel need a direct characterization of the metal uptake to determine the mechanism(s) involved in metal removal. For example, the removal of a radionuclide from solutions in contact with a sorbent material could occur by surface precipitation rather than sorption. Surfaces acting as seeds to foster the growth of secondary phases (i.e., in the case of extensive surface precipitation)[8] may not act as sorbents that remove metals via specific or outer sphere sorption mechanisms. Minimal leaching of the sorbed Sr and actinides post contact with the sorbent is important since the process subsequently washes the solids to reduce the sodium and nitrates or nitrites send to the vitrification process. Should the waste become transferred to a holding tank for long periods or need washed prior to filtration, any precipitated or weakly sorbed radionuclides may be more or less labile than specifically adsorbed or structurally incorporated radionuclides.

Basic information about the local binding environments of actinides on MST holds several benefits for the proposed large-scale process. The local (atom-scale) structural characterization of Sr and actinide associations on MST will lead toward a better predictive model of actinide loading

on MST, provide information in support of criticality safety (HLW contains fissionable actinide materials), promote the development of an improved titanate sorbent material, and create a more efficient process design with increased process throughput. Additionally, such studies may explain the relatively slow removal rates observed for some actinide species (such as with Pu) and possible competition among the radionuclides for sorption sites on MST.[7]

Researchers have studied the local structural environments of sorbed Sr and sorbed U(VI) on a variety of surfaces using X-ray based techniques.[9,10,11,12,13,14,15,16,17,18,19,20,21,22] Most of these studies examined with naturally-occurring minerals under solution conditions relevant to geologic surface and subsurface environments. The Sr K-edge X-ray absorption fine-structure (XAFS) spectroscopic techniques have also been used to study the bonding environment of sorbed Sr^{2+} species on metal oxides.[17,19 20, 21] These techniques provide average information on the local coordination environment, such as coordination numbers, radial bond distances, symmetry and oxidation state. Some Sr XAFS studies show that sorbed Sr^{2+} species on hydrous Fe oxides contains Fe in the second coordination shell—indicating that Sr sorption occurs by a specific adsorption mechanism and not by ion exchange (which we define as an outer sphere sorption because there is no metal in the second or third coordination shell of the Sr).[17,19] Others observe that sorbed Sr^{2+} on FeOOH (goethite) does not contain second shell Fe and conclude outer sphere adsorption to be operative.[20] Additionally, O'Day et al. (2000) examined the environment of sorbed Sr^{2+} in zeolite (heulandite) at Ca^{2+} (B-channel) cavity sites and observed that the sorbed Sr^{2+} existed as a hybrid species that maintained a partially-hydrated coordination sphere and had Si/Al in the second coordination shell.[19]

For U, the XAFS-based findings about the mechanism of U sorption on metal oxides vary somewhat but are more consistent than those with Sr—particularly in the neutral to high pH range. They typically indicate that sorbed UO_2^{2+} species (in the absence of a redox-active mineral surface) form inner sphere bonds with the sorbent minerals in solutions with pH values between 7 and 12.[9,12,14,15,16] Additionally, sorbed U(VI)-complexes on surfaces are usually monomeric U(VI)-hydroxo and U(VI)-carbonato species that form mono- and bidentate linkages with the participating surfaces. Dimeric U(VI) species are also observed.

Little if any experimental XAFS work has characterized sorbed Sr and U on silicotitanatesor titanates—particularly under the highly alkaline conditions that are relevant to that of HLW solutions. To elucidate the binding mechanisms of Sr and U(VI) on MST, we examined the local

structural environment of Sr and U(VI) on MST after equilibration in HLW salt simulant solutions, using synchrotron-based XAFS spectroscopic techniques. We also studied the morphology of the untreated MST and Sr-sorbed MST with high-resolution transmission electron microscopic (HR-TEM) techniques.

Experimental Procedures

MST Synthesis, Solution Preparation and Sorption Studies: The MST used in this study was made using a modified procedure to that reported by Lynch et al. (1976).[23] Testing required the preparation of two HLW simulant salt solutions containing 1.33 M NaOH, 2.6 M $NaNO_3$, 0.43 M $NaAl(OH)_4$, 0.34 M $NaNO_2$, 0.52 M Na_2SO_4 and 0.026 M Na_2CO_3 spiked individually with known levels of stable Sr and U(VI). [Prior to the addition of the U(VI), we treated the solutions with 2 g L^{-1} MST for two days and then filtered with a 0.45 μm nylon filter to remove the MST and any residue tramp Sr^{2+} from the reagent grade chemicals. Tramp Sr levels in these 5.6 M Na^+ solutions usually occur at concentrations of 0.6 mg Sr L^{-1} and this Sr is a potential competitor for sorption sites with U(VI).] The Sr and U spikes originated from nitric acid stock solutions of Sr and ^{238}U(VI) analyzed by inductively-coupled argon plasma mass spectrometry (ICP-MS) to determine the concentrations of the Sr and U in the salt solutions.

We made the Sr- and U-loaded MST samples by equilibrating 1 L of a 1 mg Sr L^{-1} salt solution (or 5 mg U(VI) L^{-1} salt solution) with known solid quantities of 0.1 to 16 g (dry weight) of MST. We stirred the mixtures for 1 week (a time period that exceeds current process flow sheet designs with MST) and filtered with a 0.45-μm nylon filter. For the Sr XAFS studies, we prepared the filtered Sr-loaded MST samples (about 0.2 g of dry solid) and analyzed as a wet paste with 0.2 mL of HLW salt solution. We dried the filtered U-containing MST solids in air at ambient temperature. After filtration, we diluted sub-samples of the U and Sr solutions in 5 M nitric acid and measured the dissolved Sr and U levels by ICP-MS to determine the amount of each Sr and U lost from solution after contact with the MST.

HR-TEM Characterization Studies. We prepared air-dried sub-samples of untreated and Sr-treated MST for analytical transmission electron microscopic examinations after embedding in EMBED-812 resin and thin-sectioning using ultramicrotomy. We estimate the section thicknesses at 50 to 70

nm. Analysis of the sections occurred using a 200 keV Hitachi HF2000 field emission and 400 keV JOEL 4000EX instruments using brightfield and darkfield imaging, selective area electron diffraction (SAED), lattice-fringe imaging, and energy-dispersive X-ray spectroscopy.

X-Ray Absorption Analyses. We collected XAFS on beamlines X23a2 and X26a at the National Synchrotron Light Source (NSLS, Brookhaven National Laboratory, Upton, NY). The Sr-XAFS data come from the Sr K-edge (16.105 keV) with the U XAFS data collected at the U L_3-edge (17.166 keV) on the prepared MST solids. We collected the XAFS data in fluorescence mode using an unfocussed X-ray beam and a fixed-exit Si(311) monochromator (X23a2, for U) or in transmission mode using a channel-cut Si(111) monochromator (X26a, for Sr). Ion chambers were used to collect incident, transmission and reference signals. Gas for the data collection in the ion chamber contained 100 % Ar (X23a2, X26a). At X23a2, we used a Lytle detector to collect fluorescence X-rays, using an Al metal foil (for Sr) or $SrCO_3$ foil (for U) to reduce background fluorescence counts. At X26A, we collected Sr XAFS in transmission using a pin diode detector. Photon flux (X23a2) was maximized with a piezo stack feedback energy stabilization system at a settling time of 0.3 seconds per change in monochromatic energy. X-ray beam sizes of 2 by 28 mm^2 (X23a2) and 350 μm^2 (X26a) were used. Strontium XAFS spectra were acquired for the Sr-loaded MST samples and several Sr reference materials [a 1 μM $SrCl_2$ solution, a 1 μM Sr^{2+} in MST-free HLW solution with the Sr form added as $SrCl_{2(s)}$, $SrTiO_{3(s)}$, $SrCO_{3(s)}$ and $Sr(NO_3)_{2(s)}$ (all from Aldrich)]. The XAFS spectra were acquired at 0.3 to 2.5 eV step intervals over a 1010 eV range, which was relative to 16.105 keV(for Sr), and over a 980 eV range, which was relative to 17.166 keV(for U). Scan limits were 120 eV less than and 760 eV greater than the U L_3-absorption edges and scan limits were 150 eV less than and 860 eV greater than the Sr K-absorption edge.

XAFS Data Analyses. The XAFS analyses included the acquisition of X-ray absorption near-edge structure (XANES) and extended X-ray absorption fine-structure (EXAFS) spectroscopic data. For the U XANES analyses, we defined the full height of the edge step for the U L_3-XANES edge energies for the U-loaded MST samples and normalized to be 0 eV with the most stable and characterized standard, $U(IV)O_{2(s)}$.[5] We also compared edge energy values for the U-loaded MST samples with that of synthetic meta-schoepite [$U(VI)O_2(OH)_2 \bullet 2H_2O$]. A relationship between

XANES edge energy value and elemental oxidation state is observed with actinides such as U, Np and Pu.[24,25]

For the EXAFS data analyses, the background contribution to the EXAFS spectra was removed using an algorithm (AUTOBK) developed by Newville et al. (1993), which minimizes *R*-space values in low *k*-space. Each chi data set was read into the WINXAS analysis package.[26,27] Replicate scans were co-added to improve S/N. For the U- and Sr-loaded MST samples and the Sr reference materials the Sr EXAFS spectra were analyzed from 2 to 14 $Å^{-1}$. Data for the $SrCO_3$ and $Sr(NO_3)_2$ solid phase standards were analyzed from 2 to 11 $Å^{-1}$. The chi data for Sr and U were k^3-weighted and Fourier-transformed (FT) to yield *R*-space.[28] Simulated EXAFS spectra were also generated based on the documented crystallographic properties for Sr and U solids using *ab initio* based theory, which involved FEFF 7.2.[29,30,31,32,33] All model fits of the EXAFS spectra were performed in *k*-space using Fourier-filtered spectra (i.e., the shell by shell method).

The first shell Sr-O fits were performed with and without a third cumulant term[19] to account for anharmonicity. O'Day et al. (2000) and Sahai et al. (2000) reviewed the use of Sr XAFS analyses to characterize atomic structural properties of Sr^{2+} in several matrices and found that the literature varies considerably due to the hydrated nature of the large divalent cation (Sr^{2+}).[19,20] Such variations were attributed to the methods used to determine amplitude reduction factors, the degree of anharmonic disorder and the number of experimental shells to be included in the model fits. To account for this, the third cumulant term has been used in fits for first shell Sr-O interactions to account for anharmonicity among light back-scattering atoms, primarily O in aqueous environments.[17,19,20] This term is often included to address the anharmonicity of hydrated Sr^{2+}.

Results and Discussion

ICP-MS Analyses. **Table 1** lists the Sr and U loading data for the samples (based on the ICP-MS analyses). Greater than 95% of the added Sr sorbed to the MST—regardless of loading. Greater than 95% of the added U(VI) sorbed to the MST (for samples UMST2 and UMST3) and 33% of the added U(VI) sorbed to the MST sample, which had the highest final loading (sample UMST1).

HR-TEM Characterization of Untreated MST and Sr-loaded MST. Little is known about the structure MST. Results from X-ray diffraction studies indicate it is highly amorphous. Scanning electron microscopy studies show that particles are spherical (snowball-like) and have a typical size

range of 5 to 12 μm.[34] MST may possess a layered structure like that of the more crystalline solid sodium nonatitanate.[35] The HR-TEM analyses with untreated MST indicate the sample has two prominent morphological populations of titanate material (**Fig. 1a** and **1b**). The first is a very fine fibrous nanocrystalline surficial material and a second is an amorphous glass-like material (compare the SAED patterns in the insets for **Fig. 1a** and **1b**).

The SAED analyses with the fibrous MST material produce the following peak intensities, which can not be assigned to known Ti phases: 0.3656-0.3144 nm (broad), 0.2577 nm, 0.2312-0.2183 nm (broad), 0.1894 nm, 0.1497 nm, 0.1404 nm, 0.1173 nm and 0.0945 nm. The basal spacing for the fibrous component of the MST is approximately 0.63 nm (**Fig. 1c**). The HR-TEM studies with Sr-sorbed MST indicate that addition of Sr to the MST (sample SrMST1) does not induce morphological changes in the MST (i.e., Sr does not facilitate the crystallization of the MST).

We only observed the added Sr (using EDS analyses, data not shown) on the fibrous portions of the MST. We did not detect sorbed Sr on the amorphous glass-like interior regions of the particles. The thickness of the fibrous surficial MST material did not change upon the addition of Sr to the MST. Additionally, the SAED pattern for the Sr-sorbed fibrous component of the MST (data not shown) remained unchanged—suggesting that the added Sr does not facilitate a conversion of the amorphous component to a more crystalline material. We did not perform HR-TEM analyses with U-sorbed MST.

Strontium XAFS Data. **Figure 2a** shows the k^3-weighted chi spectra for the three Sr-loaded MST treatments and the dilute Sr^{2+} in aqueous solution. The EXAFS data for the Sr^{2+}-loaded MST samples appear very similar. The chi data indicate the environment around the Sr^{2+} sorbed on MST differs from that of Sr^{2+} in an aqueous solution. These differences in amplitude could indicate dissimilar first-shell coordination numbers. The sample spectra for SrMST1 also indicate that the first shell distances are slightly shorter than that of the Sr^{2+} in an aqueous solution (**Fig. 2a**).

The chi data for the Sr^{2+}-loaded MST samples do not resemble that of Sr^{2+} in HLW salt simulant and in $SrCO_{3(s)}$ (data not shown). The data indicate that the Sr^{2+} in the Sr^{2+}-loaded MST samples also differs from that of Sr^{2+} in the $SrTiO_{3(s)}$. The $SrTiO_{3(s)}$ has a cubic structure and although the chi spectra appear to have light atoms (such as O) (as evidenced by an envelope at low chi which starts at 3 $Å^{-1}$ and disappears at around 8 $Å^{-1}$) (data not shown). The spectra for $SrTiO_{3(s)}$

do not resemble that of the MST samples in that there are also obvious differences in the phase and amplitude of the spectra for the Sr-loaded MST samples and the $SrTiO_{3(s)}$—in addition to that of the $Sr(NO_3)_{2(s)}$ (data not shown).

We performed first shell fits for O in *k*-space. Use of third cumulant term in the fits of the EXAFS data for the $SrCl_{2(aq)}$ solution yielded no differences in the first shell CN or R values (data not shown). However, addition of the third cumulant term in the fits for the sorbed Sr on MST did improve the first shell fits as evidenced by a lower residual and result in lower CN and *R*-values (**Table 1**). With the third cumulant term included, the first shell Sr-O radial distances for the Sr-loaded MST samples typically equaled 2.42 to 2.49 Å with CN values of 6.9 to 5.2, which indicates the Sr has a smaller coordination shell than that of the fully hydrated Sr in solution (with a CN of 9.5 as listed in **Table 1**, data not shown). A smaller CN signifies a more constrained fit, which is indicative of specific adsorption. Therefore, we anticipated outer shell Ti atoms. For the outer shells, a combination of a single second shell Sr-Ti interaction and a single third shell Sr-O interaction described the data but the most successful fits (i.e., the lowest residuals) resulted by fitting two second shell Sr-Ti interactions and a single third shell Sr-O interaction—as shown in **Fig. 2b** and listed in **Table 1**.

The EXAFS data for the two remaining Sr-loaded MST samples resemble that of the SrMST1 sample. Consequently, high quality fits resulted with the SrMST2 and SrMST3 data using two second shell Sr-Ti interactions and a single third shell Sr-O interaction (fits not shown). Model fits for Ti in the second shell of the Sr^{2+} for the remaining Sr-loaded MST samples produced similar results to that of the SrMST1 analyses as shown in **Table 1**. Fits for Ti in the second coordination shell for Sr^{2+} typically indicate the presence of two or more Ti atoms between 3.42 Å and 3.63 Å—suggesting more than one TiO_6 octahedron (**Fig. 2b**) exists in the local environment. The observation of two Ti atoms at two radial distances may indicate that an outer sphere species is also present in the local environment of the sorbed Ti.

Uranium XAFS Data. An increase with respect to the relative XANES edge energy denotes an increase in the average U oxidation state in the sample or standard of interest and a linear relationship exists between the %U(VI) in the sample and the edge energy.[24] We measured the U-XANES edge energy for the UMST sample series and expressed the value relative to that for a U(VI) standard (synthetic schoepite). The U-XANES analyses indicated U(VI) as the dominant

oxidation state of U in the MST samples (data not shown)—suggesting that no reduction of the added U(VI) occurred upon sorption to the MST. These findings agree with the EXAFS data, which indicate that the sorbed U has two O atoms at 1.8 Å, which is indicative of the uranyl [U(VI)] moiety.

Figure 3a show the k^3-weighted chi spectra for the three U-loaded MST samples. The spectra for the two samples with the highest U loadings (UMST1 and UMST2 with approximately 13,000 and 6,300 mg U kg^{-1} MST respectively) appear similar with their similarity most evident at low *k*-space. The chi data for sample UMST3 has considerably greater noise at high chi than that for the two more concentrated samples.

We Fourier filtered selected regions of the FT data and fit the EXAFS data in *k*-space using a shell by shell method. Examples of some of these fits for Sample UMST1 are shown in **Fig. 3b** and **3c**. **Table 1** shows the fit results for all of the U-containing samples. In all cases, the U-O_{ax} and U-O_{eq} radial distances and CN values are within the range of typical values expected for sorbed uranyl species. Fits for the first two selected regions in the transform (between 1.5 and 2.25 Å, uncorrected for phase shift) for UMST1 appear satisfactory.

The higher shell fits show the presence of one or more C atoms, two Ti atoms (each at different distances) and one or more U atoms in the higher shells (**Table 1**; not all data shown) and that at the highest surface loading, the sorbed U is present on average as a dimeric species. In general, fits for shells 2 and 3 proved better at high *k*-space than at low. Fits for higher shell C seemed satisfactory, but due to the similarities between the atomic weights of N and C and their somewhat similar bonding characteristics with U(VI) (i.e., bonding through bridging O atoms), we cannot exclusively determine whether N or C is associated with the U. Dissolved U(VI) has a higher affinity for C (as carbonate) than N (as nitrate).[36] Other XAFS-based characterization studies with sorbed U(VI) on minerals in near neutral basic pH solutions show that U(VI)-carbonate complexes often sorb to surfaces.[14,22] We identified second shell U (CN value of ~1) atoms and two Ti atoms (with CN values of 0.5 and 0.7) as second shell neighbor atoms in the EXAFS, indicating that U is present as a polymeric form that has an inner sphere association with the MST surface.

Simulations of binding environments for metals on perfect Ti octahedra would simply yield one type of binding site for metal sorption because the Ti-O bonds are at 90° angles and have equal bond lengths (Ti-O distances of 1.99 Å). Our Sr EXAFS results indicate multiple radial distances for the Sr-Ti interactions and hence, multiple binding sites for Sr. For sorption, these distances

must also conform to the dimensions (in 3-dimensional space) of the Ti octahedra. Elucidating such structural information about these sites might lead to an improved MST sorbent design optimized for Np, Pu, and U in addition to Sr^{2+}. Our XAFS results for U indicate that polymeric U species will sorb on MST at high U loadings. This finding indicates that on a large scale, criticality concerns need addressed if the waste contains a large amount of enriched uranium (^{235}U).

Sodium nonatitanate is a more crystalline material than MST and it has similar radionuclide uptake efficiencies as MST. Therefore, we selected a nonatitanate structure for the molecular modeling of the XAFS results to provide information on the numbers and types of binding sites that could be expected for MST—assuming that like Sr, the U(VI) also is associated with the fibrous, crystalline portion of the MST (shown in **Fig. 1a** and **1c**). Association of U with the fibrous material is likely because it is on the periphery of the MST.

Structural refinements of spectra from X-ray diffraction studies with a La-substituted nonatitanate ($LaTi_9O_{24}$) indicate there are five unique Ti octahedra,[37] four of which are distorted octahedra [Ti(1), Ti(2), Ti(4), Ti(5)] whereas one is a nearly perfect octahedron [Ti(3)]. By positioning the metals used in our studies at radial distances determined by our EXAFS studies, we determined whether the metals exhibited specific adsorption behavior (i.e., 2nd shell Ti atoms) at physically realistic binding sites with bridging O atoms on 5 possible Ti octahedra. We restricted these computer-based simulations to cases in which Ti exists in the second coordination shell in the EXAFS for U and they do not include surface associations of dimeric U species. Additionally, these simulations are based on the assumption that sorption occurs on the fibrous portions of the MST, which are on the surfaces of the MST particles.

Our first simulation examined bidentate sorption of U(VI) to a distorted Ti octahedra that is found in the $LaTi_9O_{24}$ structure.[37] The simulations indicate that the short U-Ti radial distance that obtained from the EXAFS studies can only be simulated with the Ti octahedron called Ti(4) and not with the other Ti octahedra. The model supports the radial distances for the first shell U-O_{eq} interactions generated from the fits of the EXAFS data and these data suggest that the sorption site for U(VI) is unique. Therefore, an increased number of such sites would accentuate the ability of the MST to remove dissolved U from solution.

If Sr and other actinides have little affinity for this type of site, there would be little competition between U and these actinide species for this Ti(4) site. A potential exception is that of polymeric actinide species (such as Pu colloid species or U polymeric species, which could be

bound to neighboring Ti octahedra and physically block active sites for U. Polymeric actinide species could also have a competitive affinity [with U(VI)] for that Ti(4)—according to the findings of XAFS-based characterization studies with sorbed Pu and Np on MST.[38] However, the differences in the first coordination shell structures between Pu [most likely present as Pu(IV)] and U(VI) are substantial [i.e., U(VI) typically has axial O bonds and Pu(IV) does not]. These differences in local structure may influence how close or far the Ti atoms are (radially) from the sorbing actinide. Therefore, the U-Ti distances we observe may not be applicable for sorbed Pu colloids, which are likely to have a different local structure than that of U(VI) or other hexavalent actinides.

Our last model for U(VI) sorption incorporates the sorption of U(VI) species with longer U-Ti radial distances on the surfaces of Ti octahedra Ti(1) and Ti(5) (data not shown).[37] The U-Ti distances and U-O_{eq} distances could be simulated with the association of U species on two types of distorted Ti octahedrons.

The Sr and U in this study sorbed by similar mechanisms on the MST and there is a high likelihood of sorption site specificity for these two elements. The Sr^{2+} on MST sorbs as partially-hydrated species via an inner sphere mechanism. Within the range of Sr^{2+} surface loadings studied, the coordination of the sorbed Sr remained the same regardless of loading. For sorbed U(VI), there is an influence of loading on the U speciation in that at high loadings, U sorbs primarily as a dimeric carbonato species whereas at lower loadings, U sorbs (on average) as a monomeric carbonato species. The role of the amorphous component of the MST is not known—in addition to the structure of the fibrous component, which could not be identified by diffraction analyses. However, additional studies are needed to provide that information.

Acknowledgments

This research received funding from the Tanks Focus Area DOE-EM. We thank J. Woicik of NIST, the NSLS staff for assistance and providing the approval to conduct these studies at their facility and we thank H. D. Harmon (Pacific Northwest National Laboratory, WA), M. C. Thompson (SRTC), J. U. Coughlin (WSRC) and P. C. Suggs (DOE), for their assistance, support and ideas.

Table 1. Fit results for the Sr^{-} and the U(VI)-sorbed MST samples. Values in parentheses include fits with the third cumulant term. We excluded the third cumulant term in dual (higher) shell fits due to a limited number of degree of freedom, which did not allow addition of another floating variable. Errors for first shell U-O_{axial} interactions and Sr-O are ±15 % and ±0.02 Å, errors for first shell U-$O_{equatorial}$ interactions are ±20 % and ±0.02 Å. Errors for outer shell U interactions are ±20 % and ±0.02 Å.

Sample with Elemental Concentration	Shell	Interaction	CN	R(Å)	$\sigma^2[Å]^2$
1 μM $SrCl_{2(aq)}$	1	Sr-O	9.5	2.57	0.011
SrMST1 with	1	Sr-O	7.6 (6.2)	2.55 (2.49)	0.014 (0.012)
9,000 mg Sr kg^{-1} MST	2 and 3	Sr-Ti	0.7	3.46	0.008
		Sr-O	2.2	3.92	0.006
		Sr-Ti_1	1.1	3.42	0.002
		Sr-Ti_2	0.7	3.51	0.001
SrMST2 with	1	Sr-O	7.1 (5.2)	2.55 (2.44)	0.013 (0.010)
1,800 mg Sr kg^{-1} MST	2 and 3	Sr-Ti_1	2.40	3.43	0.001
		Sr-Ti_2	2.80	3.52	0.001
SrMST3 with	1	Sr-O	9.3 (6.9)	2.53 (2.42)	0.019 (0.016)
900 mg Sr kg^{-1} MST	2 and 3	Sr-Ti_1	1.4	3.53	0.002
		Sr-Ti_2	1.2	3.63	0.001
UMST1 with	1	U-O_{ax}	2.1	1.86	0.002
7,500 mg U kg^{-1} MST		U-O_{eq}	5.0	2.41	0.007
	2 and 3	U-C	1.5	3.09	0.003
		U-Ti_1	0.5	2.97	0.001
		U-Ti_2	0.6	3.70	0.003
		U-U	1.2	3.84	0.007
UMST2 with	1	U-O_{ax}	2.6	1.84	0.003
3,000mg U kg^{-1} MST		U-O_{eq}	4.0	2.44	0.006
	2 and 3	U-C	1.1	3.24	0.010
		U-Ti	0.4	2.95	0.001
		U-Ti	0.4	3.51	0.002
		U-U	0.9	3.88	0.005
UMST3 with	1	U-O_{ax}	1.9	1.87	0.001
620 mg U kg^{-1} MST		U-O_{eq}	5.0	2.34	0.010
	2 and 3	U-C	4.1	3.29	0.010
		U-Ti	0.9	3.03	0.003
		U-Ti	0.4	3.54	0.002
		U-U	0.3	3.82	0.005

List of Figures

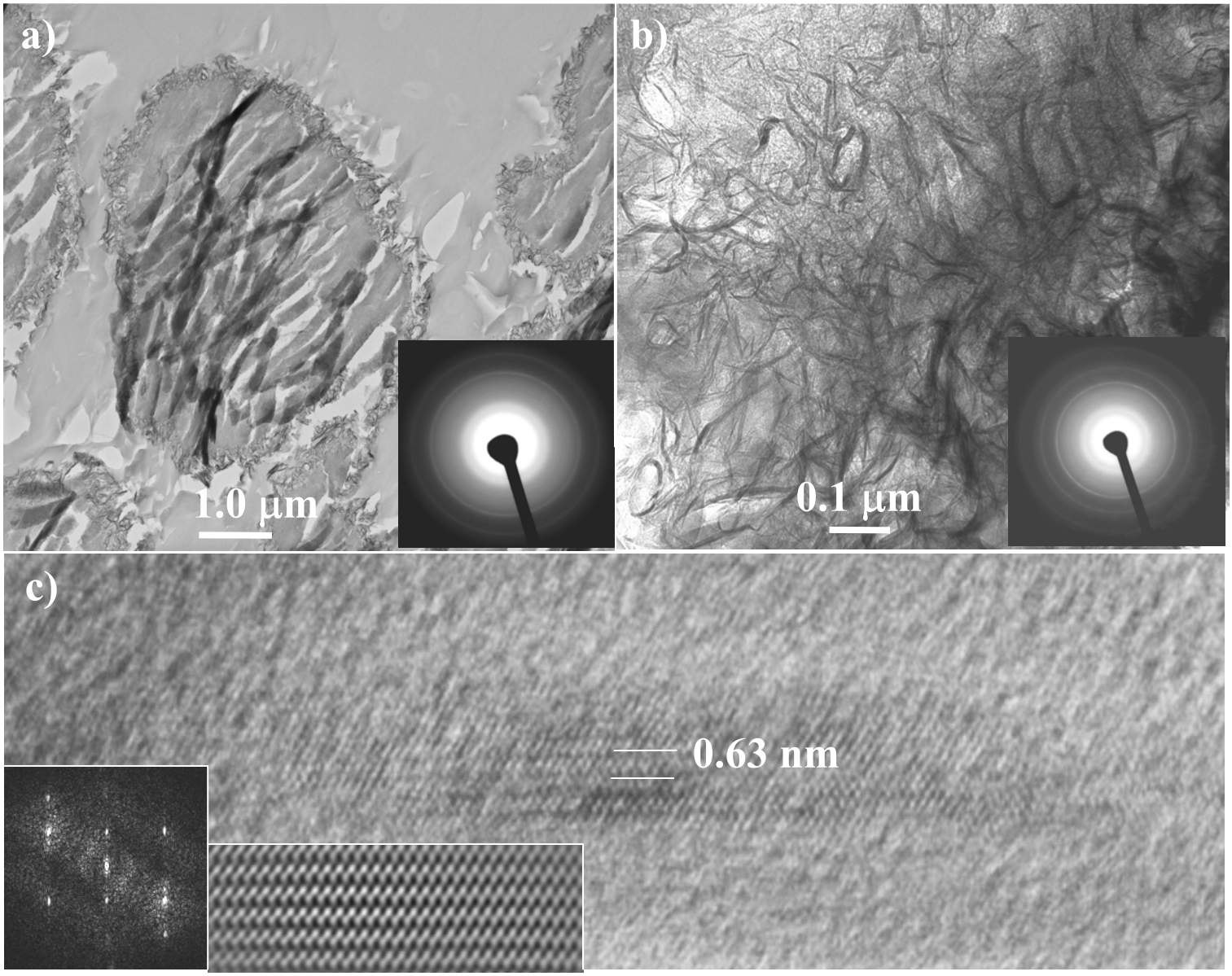
a)
1.0 μm
b)
0.1 μm
c)
0.63 nm

a)

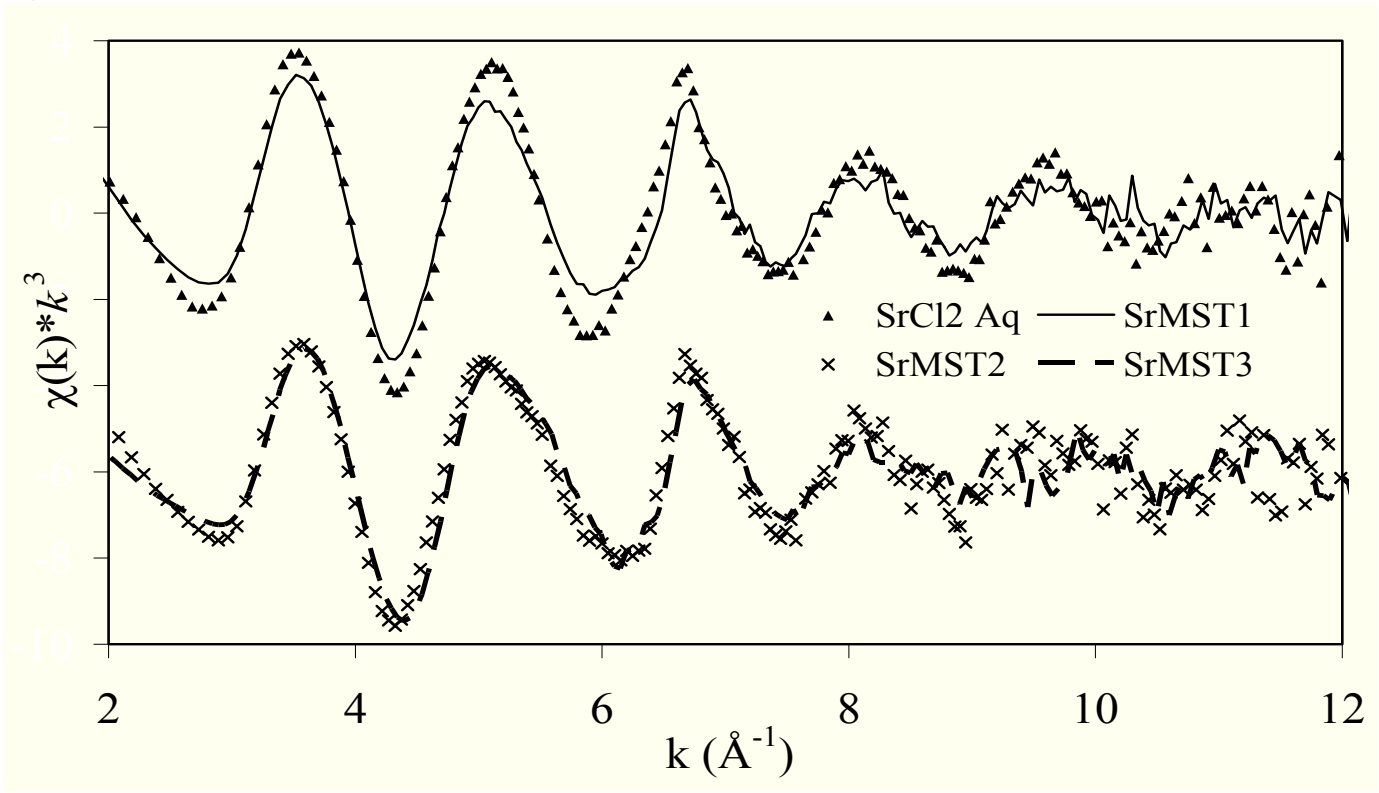
SrCl2 Aq
SrMST1
SrMST2
SrMST3
χ(k)*k3
k (Å-1)

b)

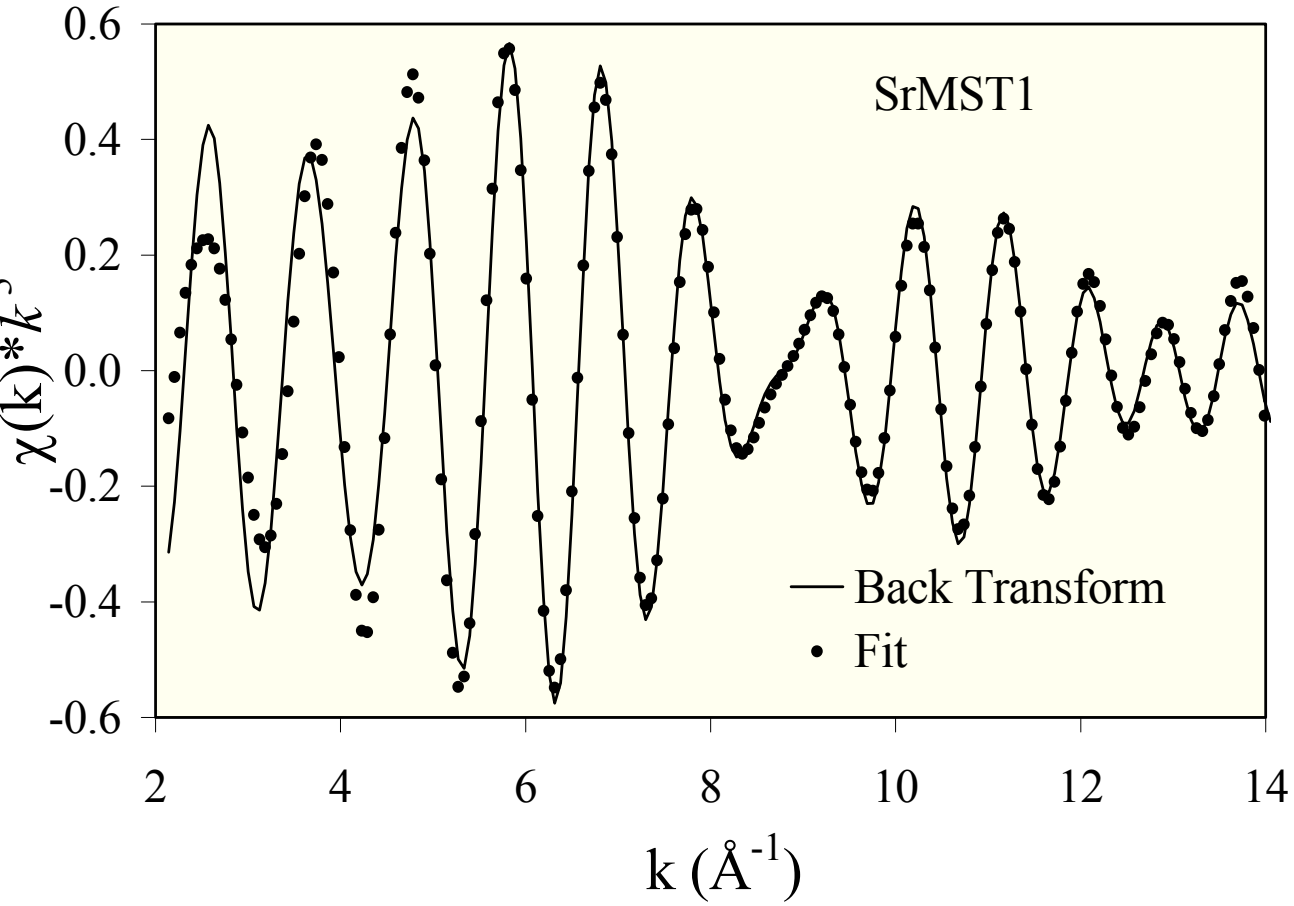
SrMST1
Back Transform
Fit
χ(k)*k3
k (Å-1)

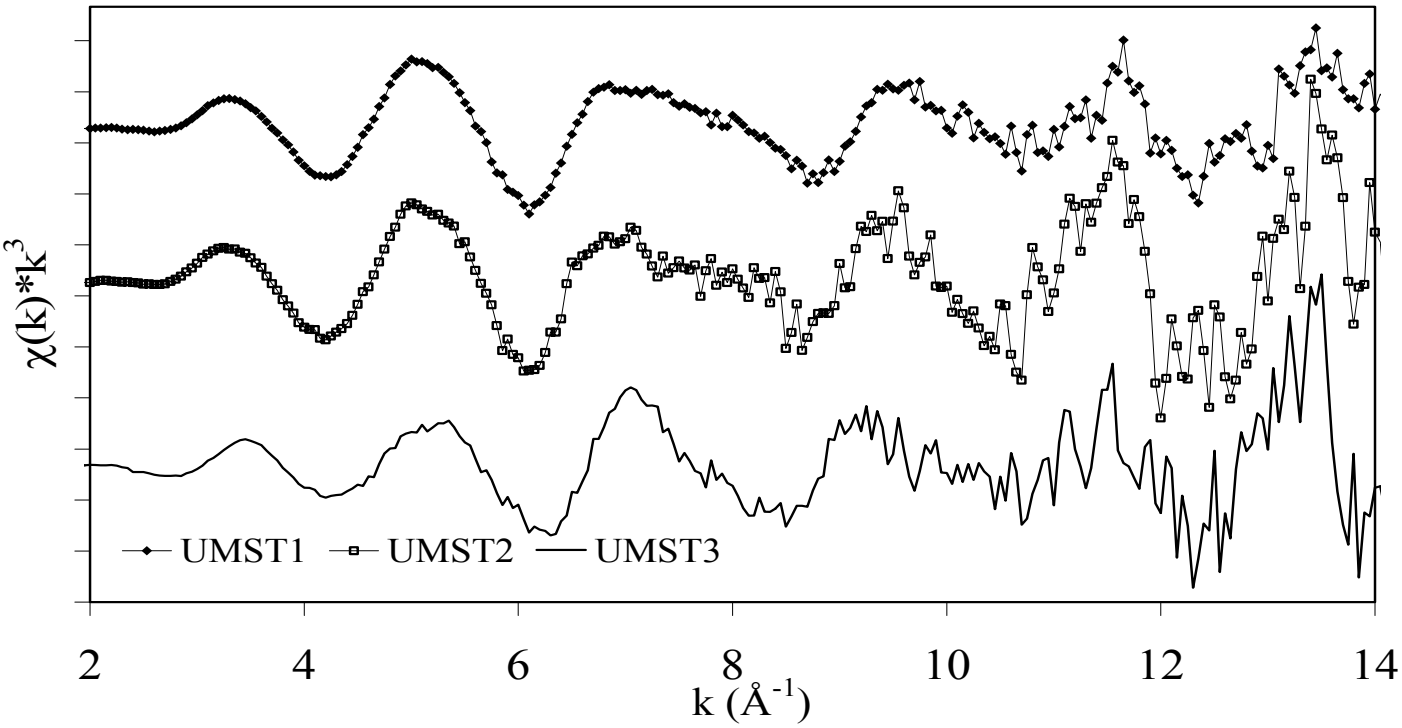
χ(k)*k3
UMST1
UMST2
UMST3
2
4
6
8
10
12
14
k (Å-1)

a)

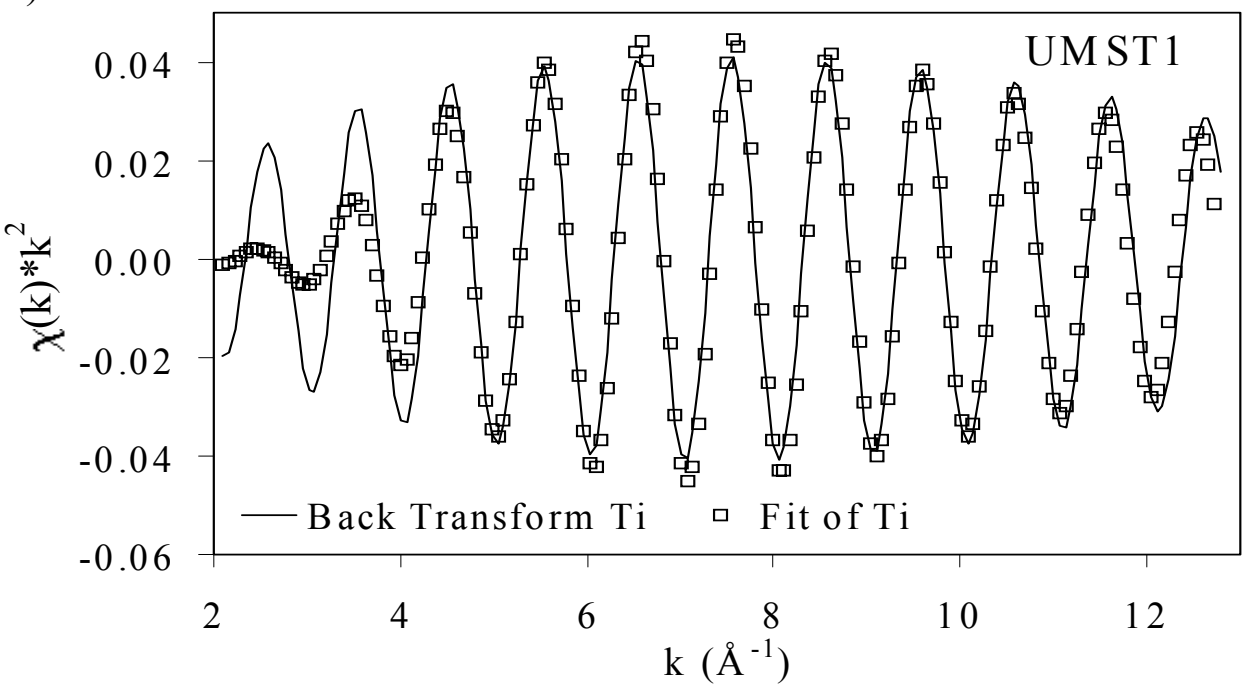
UMST1
0.04
0.02
0.00
-0.02
-0.04
-0.06
χ(k)*k2
Back Transform Ti
Fit of Ti
2
4
6
8
10
12
k (Å-1)

b)

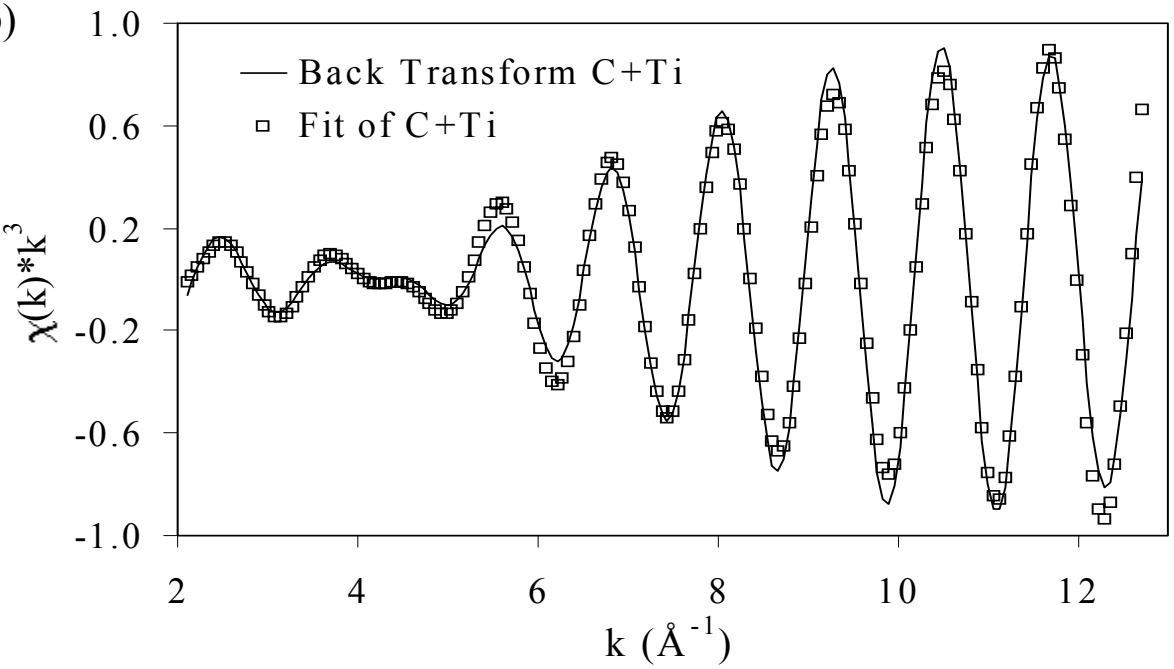
1.0
0.6
0.2
-0.2
-0.6
-1.0
χ(k)*k3
Back Transform C+Ti
Fit of C+Ti
2
4
6
8
10
12
k (Å-1)

Literature Cited

[1] Keeney-Kennicutt, W. L.; Morse, J. W. *Geochim. Cosmochim. Acta* **1985**, *49,* 2577-2588.

[2] Kohler, M.; Honeyman, B. D.; Leckie, J. O. *Radiochim. Acta* **1999**, *87*, 733-48.

[3] Combes, J.-M. et al. *Environ. Sci. Technol.* **1992**, *26*, 376-382.

[4] Turner, D. R.; Palaban, R. T.; Bertetti, F. P. *Clays and Clay Minerals* **1998**, *46*, 256-269.

[5] Duff, M. C. et al. *Environ. Sci. Technol.* **1999***, 33,* 2163-2169.

[6] Behrens, E. A.; Sylvester, P.; Clearfield, A. *Environ. Sci. Technol*. **1998**, *32,* 101-107.

[7] Hobbs, D. T.; Blume, M. S.; Thacker, H. L. Phase V simulant testing of monosodium titanate adsorption kinetics. WSRC, WSRC-TR-2000-00142, May 24, **2000**.

[8] Stumm, W. In *Chemistry of the Solid–water Interface*, Wiley, NY **1992**.

[9] Moyes, L. N.; Parkman, R. H.; Charnock, J. M.; Vaughan, D. J.; Livens, F. R.; Hughes, C. R.; Braithwaite, A. *Environ. Sci. Technol*. **2000**, *34,* 1062-1068.

[10] Hudson, E. A. et al. *Clays and Clay Minerals* **1999**, *47,* 439-457.

[11] Chisholm-Brause, C.; Conradson, S. D.; Buscher, C. T.; Eller, P. G.; Morris, D. E. *Geochim. Cosmochim. Acta* **1994**, *58,* 3625-3631.

[12] Waite, T. D., Davis, J. A.; Payne, T. E.; Waychunas, G. A.; Xu, N. *Geochim. Cosmochim. Acta* **1994**, *58*, 5465-5478.

[13] Wersin, P.; Hochella, M. F.; Persson, J.; Redden, G.; Leckie, J. O.; Harris, D. W. *Geochim. Cosmochim. Acta* **1994**, *58*, 2829-2843.

[14] Bargar, J. R.; Reitmeyer, R.; Davis, J. A. *Environ. Sci. Technol.* **1999**, *33,* 2481-2484.

[15] Sylwester, E. R.; Hudson, E. A.; Allen, P. G. *Geochim. Cosmochim. Acta* **2000**, *64*, 2431-2438.

[16] Allard, T.; Ildefonse, P.; Beaucaire, C.; Calas, G. *Chem. Geol.* **1999**, *158*, 81-103.

[17] Axe, L.; Bunker, G. B.; Anderson, P. R.; Tyson, T. A. *J. Coll. Int. Sci.* **1998**, *199*, 44-52.

[18] Axe, L.; Tyson, T. A.; Trivedi, P.; Morrison, T. *J. Coll. Int. Sci.* **2000**, *224*, 408-416.

[19] O'Day, P. A.; Newville, M.; Nuehoff, P. S.; Sahai, N.; Carroll, S. A. *J. Coll. Int. Sci.* **2000**, *222,* 184-197.

[20] Sahai, N.; Carroll, S. A.; Roberts, S.; O'Day, P. A. *J. Coll. Int. Sci.* **2000**, *222*, 198-212.

[21] Parkman, R. H.; Charnock, J. M.; Livens, F. R.; Vaughn, D. J. *Geochim. Cosmochim. Acta* **1998**, *62*, 1481-1492.

[22] Reich, T. et al., *J. Electron Spectroscopy and Related Phenomenon* **1998**, *98*, 237-243.

[23] Lynch, R. W.; Dosch, R. G.; Johnstone, J. K.; Nowak, E. J. Sandia solidification process: A broad range aqueous waste solidification process. Management of Radioactive Wastes from the Nuclear Fuel Cycle, Vol. 1, IAEA, Vienna, **1976**, p. 360-372.

[24] Bertsch, P. M.; Hunter, D. B.; Sutton, S. R.; Bajt, S.; Rivers, M. L. *Environ. Sci. Technol*. **1994**, *28,* 980-984.

[25] Conradson, S. D. et al. *Polyhedra* **1998**, *17,* 599-602.

[26] Ressler, T. *J. Synchr. Rad.* **1999**, *5*, 118-122.

[27] Newville, M.; Livins, P.; Yacoby, Y.; Rehr, J. J.; Stern, E. A. *Phys. Rev. B-Cond. Matt.* **1993,** *47,* 14126-14131.

[28] Sayers, D. E.; Bunker, B. A. In *X-ray Absorption: Techniques of EXAFS, SEXAFS and XANES.* Koningsberger, D. C. and Prins, R. (eds). Wiley, New York, Chap. 6, **1988**.

[29] Mustre de Leon, J.; Rehr, J. J.; Zabinsky, S. I.; Albers, R. C. *Phys. Rev.* **1991**, *B44*, 4146.

[30] Rehr, J. J.; Albers, R. C. *Phys. Rev.* **1990**, *B41*, 8139.

[31] Rehr, J. J.; Mustre de Leon, J.; Zabinsky, S. I.; Albers, R. C. *J. Am. Chem. Soc*. **1991**, *113,* 5135.

[32] Rehr, J. J.; Zabinsky, S. I.; Albers, R. C. *Phys. Rev. Letters* **1992**, *69,* 3397.

[33] Stern, E. A.; Newville, M.; Ravel, B.; Yacoby, Y.; Haskel, D. *Phys. B* **1995**, *208-209*, 117-120.

[34] Hobbs, D. T.; Blume, M. S.; Thacker, H. L. Screening evaluation of sodium nonatitanate for strontium and actinide removal from alkaline salt solution. WSRC, WSRC-TR-2000-00361, **2000**, Aiken, SC.

[35] Leinonen, H.; Lehto, J. *Radiochem.* **1998**, *40*, 503-506.

[36] Grenthe, I.; Fuger, J.; Konings, R.; Lemire, R. J.; Muller, A. B.; Nguyen-Trung, C.; Wanner, J. The Chemical Thermodynamics of Uranium. Elsevier Sci. Publ., New York, **1992**.

[37] Morris, R. E.; Owen, J. J.; Cheetham, A. K. *J. Phys. Chem. Solids* **1995**, *10*, 1297-1303.

[38] Duff, M. C.; Hunter, D. B.; Hobbs, D. T.; Barnes, M. J.; Fink, S. D. *Environ. Sci. Technol*. (in preparation).